3-2008

Relationship Between The Excited State Relaxation Paths Of Rhodopsin And Isorhodopsin

Angela Strambi

Pedro B. Coto

Luis Manuel Frutos

Nicolas Ferre

Massimo Olivucci
Bowling Green State University, molivuc@bgsu.edu

J|A|C|S
ARTICLES
Published on Web 02/27/2008

Relationship between the Excited State Relaxation Paths of Rhodopsin and Isorhodopsin

Angela Strambi,[†,‡] Pedro B. Coto,[†,§] Luis Manuel Frutos,[†] Nicolas Ferré,[#] and Massimo Olivucci*[,§,‡]

Dipartimento di Chimica, Università di Siena, via Aldo Moro I-53100 Siena, Italy, Instituto de Ciencia Molecular (ICMOL) Universidad de Valencia, Institutos de Paterna, 22085, ES-46071, Valencia, Spain, Laboratoire de Chimie Théorique et de Modélisation Moléculaire, UMR 6517- CNRS Université de Provence, Case 521 − Faculté de Saint-Jérôme, Av. Esc. Normandie Niemen, 13397 Marseille Cedex 20, France, and Chemistry Department, Bowling Green State University, Bowling Green, Ohio 43403

Received July 3, 2007; E-mail: olivucci@unisi.it; molivuc@bgnet.bgsu.edu

Abstract: The pigment Isorhodopsin, an analogue of the visual pigment Rhodopsin, is investigated via quantum-mechanics/molecular-mechanics computations based on an *ab initio* multiconfigurational quantum chemical treatment. The limited <5 kcal mol^{-1} error found for the spectral parameters allows for a nearly quantitative analysis of the excited-state structure and reactivity of its 9-*cis*-retinal chromophore. We demonstrate that, similar to Rhodopsin, Isorhodopsin features a shallow photoisomerization path. However, the structure of the reaction coordinate appears to be reversed. In fact, while the coordinate still corresponds to an asynchronous crankshaft motion, the dominant isomerization component involves a counterclockwise, rather than clockwise, twisting of the 9-*cis* bond. Similarly, the minor component involves a clockwise, rather than counterclockwise, twisting of the 11-*trans* bond. Ultimately, these results indicate that Rhodopsin and Isorhodopsin relax along a common excited-state potential energy valley starting from opposite ends. The fact that the central and lowest energy region of such valley runs along a segment of the intersection space between the ground and excited states of the protein explains why the pigments decay at distinctive conical intersection structures.

1. Introduction

The visual pigment Rhodopsin[1,2] (Rh) is a G-protein-coupled receptor containing an 11-*cis*-retinal chromophore (PSB11) bound to a lysine residue (Lys296) via a protonated Schiff base linkage (see green substructure in Figure 1). While the biological activity of Rh is triggered by the light-induced 11-*cis* → *all-trans* isomerization of PSB11, this reaction owes its efficiency (e.g., short time scale and high quantum yield) to the protein cavity.[1] Indeed, computational and experimental studies[3−5] have shown that, in the apoprotein (opsin), PSB11 isomerizes to a distorted *all-trans*-retinal (PSBT) identified as the chromophore of the first isolable ground state photocycle intermediate Bathorhodopsin (bathoRh).

Isorhodopsin (isoRh) is a Rh analogue featuring a 9-*cis*-retinal chromophore (PSB9) embedded in the same opsin environment. It has been shown that isoRh can activate a weaker visual response[6] triggered by a light-induced 9-*cis* → *all-trans* isomerization of PSB9 featuring a longer time-scale[7] and a reduced quantum yield.[8] Remarkably, as first reported by Yoshizawa and Wald,[9] the photoisomerization of isoRh results in the production of the same bathoRh intermediate obtained from Rh.

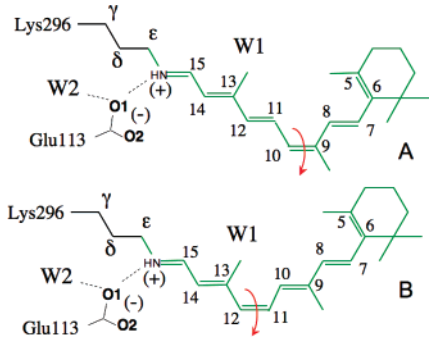

Figure 1. Schematic structure of the chromophores (in green) of the visual receptor (A) Isorhodopsin and (B) Rhodopsin. The curved arrows indicate the reactive double bonds.

[†] Dipartimento di Chimica, Università di Siena.
[‡] Chemistry Department, Bowling Green State University.
[§] Instituto de Ciencia Molecular (ICMOL) Universidad de Valencia.
[#] Laboratoire de Chimie Théorique et de Modélisation Moléculaire, UMR 6517- CNRS Université de Provence.

(1) Mathies, R. A.; Lugtenburg, J. In *Handbook of Biological Physics*; Stavenga, D. G., Ed.; Elsevier: New York, 2000; Vol. 3.
(2) Kandori, H.; Shichida, Y.; Yoshizawa, T. *Biochemistry (Moscow)* **2001**, *66*, 1197−1209.
(3) Warshel, A. *Nature* **1976**, *260*, 679−683.
(4) Honig, B. *Annu. Rev. Phys. Chem.* **1978**, *29*, 31−57.
(5) Birge, R. R. *Annu. Rev. Biophys. Bioeng* **1981**, *10*, 315−354.
(6) Fan, J.; Rohrer, B.; Moiseyev, G.; Ma, J.; Crouch, R. K. *Proc. Natl. Acad. Sci. U.S.A.* **2003**, *100*, 13662−13667.
(7) Schoenlein, R. W.; Peteanu, L. A.; Wang, Q.; Mathies, R. A.; Shank, C. V. *J. Phys. Chem.* **1993**, *97*, 12087−12092.
(8) Hurley, J. B.; Ebrey, T. G.; Honig, B.; Ottolenghi, M. *Nature* **1977**, *270*, 540−542.
(9) Yoshizawa, Y.; Wald, G. *Nature (London)* **1963**, *197*, 1279−1286.

10.1021/ja0749082 CCC: $40.75

Indeed, it has been shown that Rh, bathoRh and isoRh form, upon irradiation, a three-component photoequilibrium.[10,11]

Below, we show that the fact that Rh and isoRh can be photochemically converted to the same ground state intermediate provides the opportunity to expand our understanding of the structure of the excited-state potential energy surface of visual pigments. Indeed, it is apparent that the distinct photochemical reaction paths of Rh and isoRh (i.e., an approximate minimum energy path—see Section 2 for details—connecting Franck−Condon points on the excited-state energy surface to product valleys on the ground state energy surface) must describe converging excited-state relaxations ultimately leading to the same ground state energy minimum. Furthermore, the comparison of the computed PSB11 and PSB9 reaction paths must provide information on the apoprotein control of the geometrical deformation of the chromophore.

Previous computational studies[12] on Rh indicate that the level of theory required for a quantitative description of the geometrical and electronic structure of its chromophore must include the treatment of electron dynamic correlation. In particular, the use of a quantum-mechanics/molecular-mechanics (QM/MM) model based on a QM *ab initio* multiconfigurational second-order perturbation theory, allows for a comparison with the observed spectra. Indeed, we have shown: (i) that for a Rh model (**S_0-Rh**) derived from monomer A of the X-ray structure of bovine Rh, the CASPT2//CASSCF/6-31G*/AMBER protocol[13] yields a PSB11 conformation consistent with the experiment;[14,15] (ii) that the protocol also yields a bathoRh model (**S_0-I**)[13] with a PSBT structure close to the one recently resolved via femtosecond Raman spectroscopy[16] (this is comparable with the one recently reported by Okada and co-workers[17,18]); and (iii) that, again, the same protocol has been shown to reproduce the λ^a_{max} change for a small set of modified rhodopsins.[19] The **S_0-Rh** model also features $S_0 \rightarrow S_1$ and $S_0 \rightarrow S_2$ λ^a_{max} values (478 and 327 nm) 3 kcal mol^{-1} off the experimental values (498 and 340 nm),[8] a computed 14.6 D change in dipole moment ($\Delta\mu$) that falls within the observed 13−15 D range[20] and a $S_0 \rightarrow S_1$ oscillator strength value (0.8) that compares well with the experimental quantity (1.0).[8] Similarly, the computed λ^a_{max} and photon energy storage of bathoRh are 5 kcal mol^{-1} off the observed values. The method has also been used to evaluate the λ^a_{max} of PSB11 in methanol yielding an opsin-shift 2 kcal mol^{-1} off of the experimental value.[13] We found that the $S_0 \rightarrow S_1$ λ^a_{max} computed with the ANO-S (C,N[4s3p1d]/H[2s]) correlated basis set yields a reduced 10 nm red-shifted error.[19] However, due to its excessive computational cost, such a basis could not be adopted here.

Recently, we have reported the CASPT2//CASSCF/6-31G*/AMBER excited state (S_1) reaction path that connects the Franck−Condon structure **S_0-Rh** to an excited state/ground state conical intersection structure **Rh−CI** featuring a highly twisted (∼80°) reactive C_{11}═C_{12} bond.[13,21] Such conical intersection provides the mechanistic entity allowing for fully efficient decay of the photoexcited chromophore to the ground state (S_0) and, ultimately, for bathoRh production. We have also shown that trajectory computations with a scaled-CASSCF/6-31G*/ AMBER potential that reproduces the **S_0-Rh → Rh−CI** reaction path, indicate that $S_1 \rightarrow S_0$ decay must take place on a ∼120 fs time scale in line with the experiment.[21] Comparison of the reaction coordinate associated with the **S_0-Rh → Rh−CI** reaction path with the trajectory reveals that the molecular motion associated with the space-saving excited-state isomerization of PSB11, an asynchronous crankshaft (or bicycle pedal) deformation of the $-C_9$═$C_{10}-C_{11}$═$C_{12}-$ moiety (see Figure 1 for the atom numbering), is also present along the **S_0-Rh → Rh−CI** reaction coordinate and is thus driven by the shape of the S_1 potential energy surface.[21]

In the present work, we compute, using the same CASPT2//CASSCF/6-31G*/AMBER protocol, the S_1 reaction path driving the isomerization of isoRh. Accordingly, we build and validate a suitable **S_0-isoRh** model, compute and analyze the reaction coordinate associated to the photoisomerization process, and compare it with the **S_0-Rh → Rh−CI** of Rh. We show that the structural differences of the isoRh and Rh paths provide information on the role of the protein cavity in the **S_1** and (indirectly) **S_0** relaxation of PSB11 and PSB9.

2. Methodology

Our QM/MM scheme is fully described in ref 22. Briefly, the method is based on a hydrogen link-atom[23] and electrostatic embedding[3] schemes with the frontier placed at the $C_\delta-C_\epsilon$ bond of the Lys296 side chain (see Figure 1). The *ab initio* QM calculations are based on a CASPT2//CASSCF/6-31G* methodology. The active space comprises the full π-system of PSB11 (12 electrons in 12 π-orbitals). The MM (we use the AMBER force field) and QM segments interact in the following way: (i) all QM atoms feel the electrostatic potential of the MM point charges; (ii) stretching, bending, and torsional potentials involving at least one MM atom are described by the MM potential; and (iii) QM and MM atom pairs separated by more than two bonds interact via either standard or re-parametrized[24,25] van der Waals potentials. CASSCF/6-31G*/AMBER geometry optimization is carried out with the GAUSSIAN03[26] and TINKER[27] programs. The construction of the **S_0-Rh**, **S_0-isoRh**, and **S_0-I** featuring PSB11, PSB9, and PSBT chromophores, respectively, has been documented.[19,22] All protein models used in the computation are derived from monomer A deposited in the PDB archive as file 1HZX[15]. (For isoRh, no archived crystallographic structure is currently available. Thus, we assume

(10) Schick, G. A.; Cooper, T. M.; Holloway, R. A.; Murray, L. P.; Birge, R. R. *Biochemistry* **1987**, *26*, 2556−2562.
(11) Hug, S. J.; Lewis, J. W.; Kliger, D. S. *J. Am. Chem. Soc.* **1988**, *110*, 1998−1999.
(12) Wanko, M.; Hoffmann, M.; Strodel, P.; Koslowski, A.; Thiel, W.; Neese, F.; Frauenheim, T.; Elstner, M. *J. Phys. Chem. B* **2005**, *109*, 3606−3615.
(13) Andruniów, T.; Ferré, N.; Olivucci, M. *Proc. Natl. Acad. Sci. U.S.A.* **2004**, *101*, 17908−17913.
(14) Verdegem, P. J. E.; Bovee-Geurts, P. H. M.; Grip, W. J. d.; Lugtenburg, J.; Groot, H. J. M. d. *Biochemistry* **1999**, *38*, 11316−11324.
(15) Teller, D. C.; Okada, T.; Benke, C. A.; Palczewski, K.; Stenkamp, R. E. *Biochemistry* **2001**, *40*, 7761−7772.
(16) Kukura, P.; McCamant, D. W.; Yoon, S.; Wandshneider, D. B.; Mathies, R. A. *Science* **2005**, *310*, 1006−1009.
(17) Nakamichi, H.; Okada, T. *Angew. Chem., Int. Ed.* **2006**, *45*, 4270−4273.
(18) Schreiber, M.; Sugihara, M.; Okada, T.; Buss, V. *Angew. Chem., Int. Ed.* **2006**, *45*, 4274−4277.
(19) Coto, P. B.; Strambi, A.; Ferré, N.; Olivucci, M. *Proc. Natl. Acad. Sci. U.S.A.* **2006**, *103*, 17154−17159.
(20) Mathies, R. A.; Stryer, L. *Proc. Natl. Acad. Sci. U.S.A.* **1976**, *73*, 2169−2173.
(21) Frutos, L. M.; Andruniów, T.; Santoro, F.; Ferré, N.; Olivucci, M. *Proc. Natl. Acad. Sci. U.S.A.* **2007**, *104*, 7764−7769.
(22) Ferré, N.; Olivucci, M. *J. Am. Chem. Soc.* **2003**, *125*, 6868−6869.
(23) Singh, U. C.; Kollman, P. A. *J. Comput. Chem.* **1986**, *7*, 718−730.
(24) Ferré, N.; Olivucci, M. *Theochem* **2003**, *632*, 71−82.
(25) Ferré, N.; Cembran, A.; Garavelli, M.; Olivucci, M. *Theor. Chem. Acc.* **2004**, *112*, 335−341.

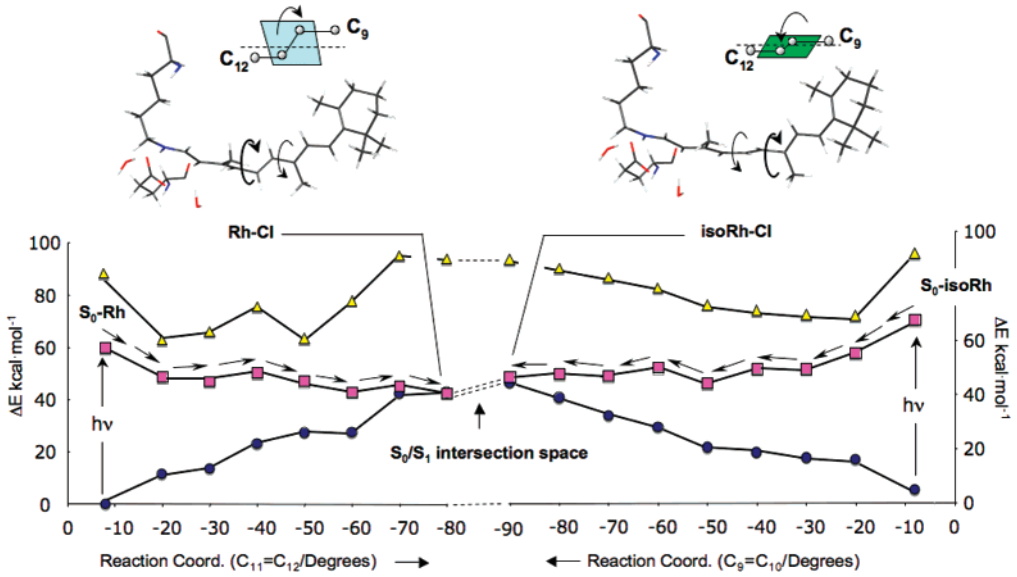

Figure 2. CASPT2//CASSCF/6-31G*/AMBER energy profiles in the spectroscopic (S_1) state along the **S_0-Rh** (left diagram, see ref 21) and the **S_0-isoRh** (right diagram) reaction paths (squares). The energies of the ground (S_0) and second excited state (S_2) are also reported along the same paths (circles and triangles, respectively). The structures of the conical intersection channels delimiting the intersection space (schematically indicated by a double dashed line) are given on the top of the diagrams. The α plane is the plane that contains (roughly) the nearly planar $-C_9-C_{10}-C_{11}-C_{12}-$ skeletal segment.

that its average protein cavity is similar to that of Rh.) With the exception of the Glu113 counterion (forming a salt-bridge with NH(+)), the opsin cavity is set neutral consistently with the experiment.[28] While the protein is kept frozen during the optimizations (given the subpicosecond excited-state evolution of the chromophore, a fixed-opsin approximation seems to be adequate), the Lys296 side chain, the position/orientation of two TIP3P water molecules (W1 and W2 in Figure 1) and the chromophore (PSB11 and PSB9 for Rh and isoRh, respectively) are relaxed. The optimizations were stopped when the maximum force is <0.0015 u.a./bohr and the rms force is <0.0010 u.a./bohr. Due to the excessive computational cost, no second derivative computations could be performed to rigorously determine the nature of the stationary points. At the equilibrium geometries, a single point three-root CASPT2 calculation with a three-root state averaged CASSCF reference wavefunction is carried out using the MOLCAS-6.4[29] program to evaluate the λ_{max} and the oscillator strength (f) of the $S_0 \rightarrow S_1$ and $S_0 \rightarrow S_2$ transitions. The AMBER charges account for S_0 polarization effects in a mean-field way.[30] The same charges are used for the excited-state computations with no ad hoc dielectric constant added. Recently, two better resolved crystallographic structures of Rh (1L9H[31] at 2.6 Å and 1U19[32] at 2.2 Å in the PDB archive) have become available. The new structures display a position of W2 that differs significantly from that defined in our original model. Thus, in order to test the sensitivity of the spectral parameters to water re-location, we also reconstruct and test the **S_0-Rh**, **S_0-isoRh**, and **S_0-I** models using the 1U19 crystallographic structure (see also ref 33). In all cases, the excitation energies and wavelengths are evaluated in terms of the energy gap between the corresponding electronic states. The S_1 reaction coordinates defining the two reaction paths discussed below are computed starting from the **S_0-Rh** and **S_0-isoRh** structures as follows. First, a chromophore unconstrained geometry optimization is carried out in the excited-state generating two excited-state relaxed structures. Second, starting at these relaxed structures, a relaxed scan along the reactive $C_{11}=C_{12}$ (for Rh) and $C_9=C_{10}$ (for isoRh) bond torsional coordinates (i.e., $C_{10}-C_{11}-C_{12}-C_{13}$ and $C_8-C_9-C_{10}-C_{11}$ dihedral angles) is computed with a step of −10°. Such a protocol, based on a relaxed scan rather than on a steepest-descent path computation, has been used to overcome convergence problems related with the flatness of the S_1 energy surface along the dominating $C_{10}-C_{11}-C_{12}-C_{13}$ and $C_8-C_9-C_{10}-C_{11}$ dihedral angles. The resulting reaction paths are considered mechanistically valid approximations of S_1 minimum energy paths. In fact, for Rh, the validity of the computed paths has been assessed by comparison with a recently reported unconstrained S_1 trajectory[21] computed using the same Rh model and level of theory. The comparison shows that the structural evolution described by the trajectory and by the reaction path is substantially the same.

The reaction paths defined above are computed in the field of the fixed crystallographic structure of the protein (with the exception of Lys296). Such a field affects the computed paths through the van der Waals interactions between protein and chromophore centers and the electrostatic interaction between protein centers and the chromophore electron density (see point i above). This approximation seems to be adequate if one considers that the S_1 evolution is completed on a subpicosecond time-scale.

3. Results and Discussion

3.1. Energy Profiles. In Figure 2, we report the energy profile of the S_1 reaction paths computed starting from **S_0-Rh** (left) and **S_0-isoRh** (right) energy minima. In the same figure, we

(26) Frisch, M. J.; et al. *Gaussian 03*, revision C.02; Gaussian, Inc.: Wallingford, CT, 2004.
(27) Ponder, J. W.; Richards, F. M. *J. Comput. Chem.* **1987**, *8*, 1016−1024.
(28) Fahmy, K.; Jager, F.; Beck, M.; Zvyaga, T. A.; Sakmar, T. P.; Siebert, F. *Proc. Natl. Acad. Sci. U.S.A.* **1993**, *90*, 10206−10210.
(29) Karlström, G.; Lindh, R.; Malmqvist, P.-Å.; Roos, B. O.; Ryde, U.; Veryazov, V.; Widmark, P.-O.; Cossi, M.; Schimmelpfennig, B.; Neogrády, P.; Seijo, L. *Comput. Mater. Sci.* **2003**, 28.
(30) Besler, B.; Merz, K.; Kollman, P. *J. Comput. Chem.* **1985**, *11*, 431−439.
(31) Okada, T.; Fujiyoshi, Y.; Silow, M.; Navarro, J.; Landau, E. M.; Shichida, Y. *Proc. Natl. Acad. Sci. U.S.A.* **2002**, *99*, 5982−5987.
(32) Strambi, A.; Coto, P. B.; Ferré, N.; Olivucci, M. *Theor. Chem. Acc.* **2007**, *118*, 185−191.
(33) Okada, T.; Sugihara, M.; Bondar, A. N.; Elstner, M.; Entel, P.; Buss, V. *J. Mol. Biol.* **2004**, *342*, 571−583.

also report the S_0 and S_2 energy profiles computed along the S_1 paths. In both cases, the initial relaxation (from $-10°$ to $-20°$), leading to a rapid $\sim$15 kcal mol^{-1} energy decrease, is largely dominated by a stretching mode corresponding to the inversion of the bond order along the chromophore backbone (double-bond expansion and single-bond contraction). This initial change has been previously reported,[13] and it is connected with the positive charge translocation from the $-C_{14}=N-$ region toward the β-ionone ring. The stretching relaxation is completed at the $-20°$ structures and remains unchanged after these points. It is apparent from inspection of Figure 2, that, in both cases, the force field driving the subsequent isomerization is flat and connects the Franck−Condon points to a S_0/S_1 conical intersection (a real crossing between electronic states of the same spin multiplicity). Since the intersections provide a fully efficient decay channel, the energy surface is consistent, for both pigments, with the observed subpicosecond excited-state lifetime. However, a closer look reveals that, while in Rh the conical intersection (i.e., the **Rh−CI** structure) is reached when the isomerizing $C_{11}=C_{12}$ double bond is between $-70°$ and $-80°$ twisted, in isoRh the energy degeneracy is only intercepted when the reactive double bond is $-90°$ twisted (**isoRh-CI**). Furthermore, while the Rh energy profile features a flat $-30°$ energy minimum, the corresponding isoRh intermediate is shifted to the $-50°$ region and features a higher ($\sim$6 kcal mol^{-1}) barrier. The origin of these minima (and of the related barriers) may be associated to a change in character of the reaction coordinates that display a rapid change in the $C_9=C_{10}$, $C_{13}=C_{14}$ and $C_{11}=C_{12}$, $C_{13}=C_{14}$ torsions for Rh and IsoRh, respectively. However, an analysis of the S_1 energy profile of isoRh, in terms of protein−chromophore van der Waals and electrostatic interactions, indicates that the latter determine the depth of the $-50°$ minimum (see Sections 8 and 9 in the Supporting Information).

One remarkable feature documented in Figure 2 is related to the intersection points. In fact, the S_0, S_1, and S_2 energy profiles developing from the very different **S_0-Rh** and **S_0-isoRh** Franck−Condon structures, seem to merge after the intersection regions are reached (i.e., at $-80°/-90°$ twisting of the corresponding reactive bonds). This indicates that the S_1 potential energy valleys controlling the isomerization of Rh and isoRh join, from different directions, a common energy surface region characterized by the degeneracy of the S_0 and S_1 states. This region belongs to the S_0/S_1 intersection space, that is the *n*-2-dimensional space (*n* being the number of vibrational degrees of freedom of the system) of electronic energy degeneracy.[34,35] This conclusion is reinforced by inspection of the distinct **Rh−CI** and **isoRh−CI** chromophore structures (see Figure 2, top). As detailed in Figure 3, a superposition of these structures demonstrates that they are similar, with the largest differences corresponding to the orientation of a nearly planar $-C_9=C_{10}-C_{11}=C_{12}-$ segment (on S_1 $-C_{10}-C_{11}-$ has a double bond character) of the carbon backbone. Such a segment is found to be substantially planar also at the common **S_0-I** intermediate. Of course, the C_8 and C_{13} centers do not lie on such plane. In fact, the values of the $C_8-C_9-C_{10}-C_{11}$ and $C_{10}-C_{11}-C_{12}-C_{13}$ dihedral angles are $-90°$ and $-155°$ and $-161°$ and $-80°$ for **isoRh−CI** and **Rh−CI** respectively. Consistently, the $C_9-C_{10}-C_{11}-C_{12}$ dihedral is close to planarity (187° and 176° for the two pigments respectively). As illustrated in Figure 3, the planes (α and β) containing the $-C_9=C_{10}-C_{11}=C_{12}-$ moiety in the two intersections are nearly orthogonal.

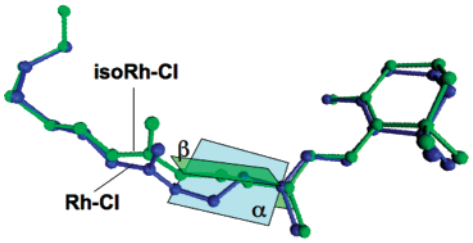

Figure 3. CASSCF/AMBER structures for the conical intersections of Rh and isoRh. The planes α and β show the mutual orientation of the $-C_9=C_{10}-C_{11}=C_{12}-$ segment in **Rh−CI** and **isoRh−CI**, respectively. The same planes are reported on the structures of Figure 2.

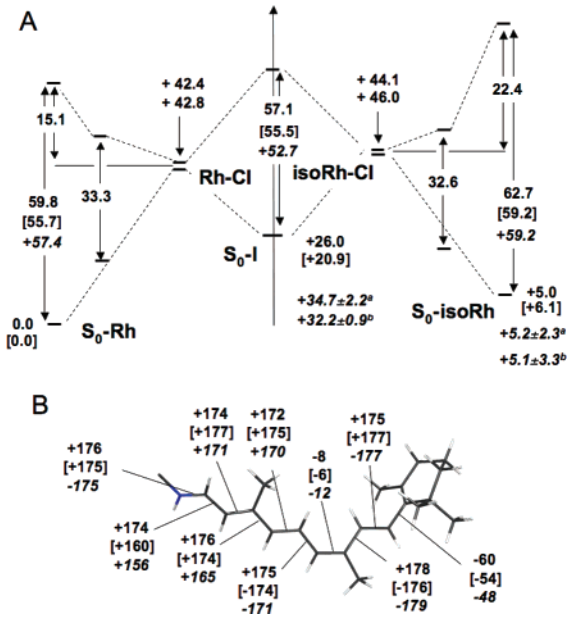

Figure 4. A. CASPT2//CASSCF/6-31G*/AMBER $S_0 \rightarrow S_1$ excitation energies (double arrows) and S_0 relative energies (kcal mol^{-1}) computed for the **S_0-Rh**, **S_0-isoRh**, **Rh−CI**, **isoRh−CI** and **S_0-I** structures. The observed quantities (in italics) are from (a) ref 39 and (b) ref 10 for energetics and refs 40 and 41 for absorption. B. CASSCF/AMBER/6-31G* optimized isoRh structure **S_0-isoRh**. The geometrical parameters are given in degrees. The quantities in square brackets refer to models based on the 1U19 crystallographic structure. The observed values (see Supporting Information for further details) are in italics.

The accuracy of the results reported above can be assessed inspecting the energy diagram reported in Figure 4A and the **S_0-isoRh** structure reported on Figure 4B. It is apparent that the excitation energies computed for the **S_0-Rh**, **S_0-isoRh**, and **S_0-I** models are reproduced within 4 kcal mol^{-1} when the protein model is based on the 1HZX crystallographic structure (this is the one used for the reaction path mapping). The difference with respect to the experiment decreases only 1 kcal mol^{-1} when using the more accurate 1U19 crystallographic structure. The computed geometrical parameters of the previously reported **S_0-isoRh** model match well the experimentally derived structure of the isoRh chromophore.[36,37] The previously reported differences between the computed and observed geometrical param-

(34) Atchity, G. J.; Xantheas, S. S.; Ruendeberg, K. J. *J. Chem. Phys.* **1991**, *95*, 1862−1876.
(35) Yarkony, D. R. *Rev. Mod. Phys.* **1996**, *68*, 985−1013.
(36) Nakamichi, H.; Okada, T. *Photochem. Photobiol.* **2007**, *83*, 232−235.
(37) Sekharan, S.; Sugihara, M.; Weingart, O.; Okada, T.; Buss, V. *J. Am. Chem. Soc.* **2007**, *129*, 1052−1054.

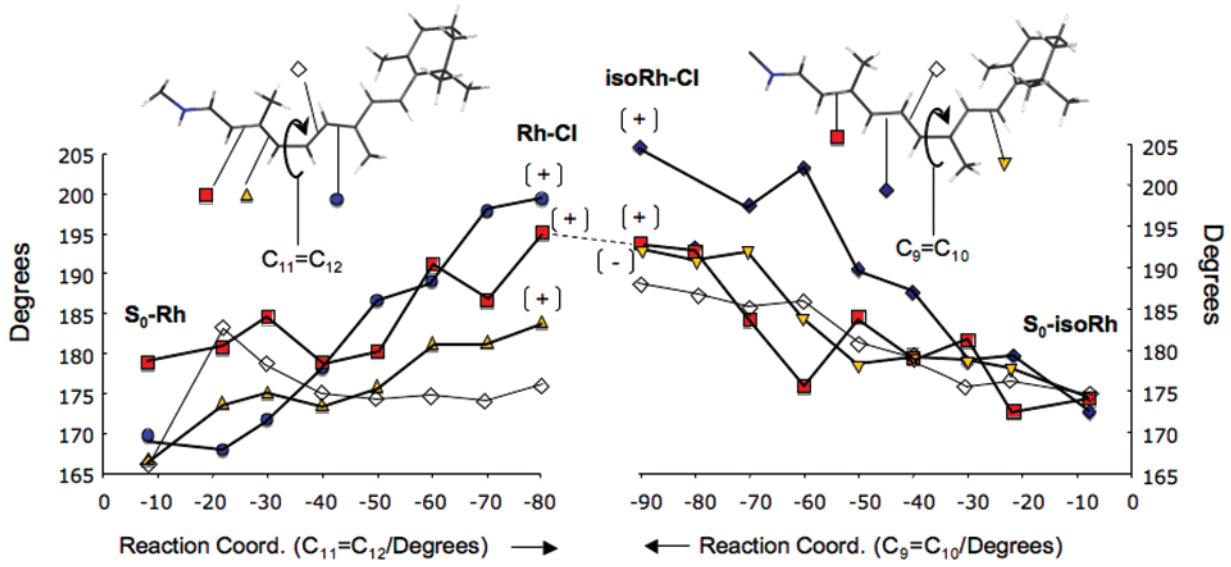

Figure 5. Variation of the relevant backbone torsions of the S_1 retinal chromophore along (left) the **S_0-Rh** and (right) the **S_0-isoRh** reaction paths computed as relaxed scans driven by the C_{11}=C_{12} and C_9=C_{10} torsion respectively and starting from the **S_0-Rh** and **S_0-isoRh** equilibrium structures.

Table 1. Franck−Condon to Conical Intersection Differences in the Dihedral Angles of the Rh and IsoRh Chromophores

IsoRh	Rh
$C_9-C_{10} \cong -82°$	$C_{11}-C_{12} \cong -72°$
$C_{11}-C_{12} \cong +32°$	$C_9-C_{10} \cong +30°$
$C_{13}-C_{14} \cong +19°$	$C_{13}-C_{14} \cong +16°$
$C_7-C_8 \cong -17°$	$C_{12}-C_{13} \cong +30°$

eters of Rh[13,21] are of the same magnitude. While, as expected, the **S_0-isoRh** is located above the **S_0-Rh** and its computed relative stability appears to be insensitive to the choice of the opsin model (i.e., 1HZX vs 1U19), the stability of the bathoRh model appears to be 6 kcal mol^{-1} off the available experimental value and it is also quite sensitive to the opsin model used in the computation (the 1HZX and 1U19 models mainly differ for the location of the internal water W2. See also ref 33).

3.2. Reaction Coordinate. As mentioned above, S_1 trajectory computations have shown that, in Rh, a *counterclockwise* crankshaft rotation of the $-C_9$=$C_{10}-C_{11}$=$C_{12}-$ moiety (i.e., of plane α in Figure 2 and 3) starting 60 fs after photon absorption characterizes the evolution and $S_1 \rightarrow S_0$ decay of the retinal chromophore. Consistently with the **Rh−CI** structure discussed above, this type of structural change is also found in the Rh reaction coordinate. This can be seen in Figure 5 (left) where we report the change in dihedral angles as a function of the $C_{10}-C_{11}-C_{12}-C_{13}$ dihedral of the reacting (C_{11}=C_{12}) double bond. Indeed it can be seen that starting at −40°, the $C_9-C_{10}-C_{11}-C_{12}$ angle remains almost unchanged at values close to planarity (∼175°) while the reaction coordinate undergoes a further −40° decrease reaching the intersection at −80°. In contrast, the adjacent C_8-C_9=$C_{10}-C_{11}$ angle rotates of +20° before the intersection is reached. The −40 °C_{11}=C_{12} torsional change combined with the +20 °C_9=C_{10} change is consistent with an asynchronous counterclockwise rotation of plane α. Indeed, similar to Rh, it can be seen that starting at −60°, twisting the $C_9-C_{10}-C_{11}-C_{12}$ angle of isoRh remains almost unchanged at a near 185° value, whereas its C_{11}=C_{12} bond undergoes a +15° rotation. The combination of the −30° torsion of the reacting C_9=C_{10} bond and of the +15° torsion of the C_{11}=C_{12} bond results, again, in an asynchronous rotation of plane α but in the clockwise direction. This inverse behavior is illustrated by the pair of curved arrows on the **Rh−CI** and **isoRh−CI** structures of Figure 2. Not only the nature of the $-C_9$=C_{10}/C_{11}=$C_{12}-$ segment rotation appears to be reversed, but also the ∼2:1 (i.e., −40°:+20°) ratio of the C_9=C_{10} and C_{11}=C_{12} bond deformations of Rh becomes a ∼1:2 (i.e., +15°:−30°) ratio in isoRh. Such a reversed ratio has been previously described.[38] In other words, not only the direction of rotation of the plane is reversed, but also the degree of synchronicity of the torsions delimiting it.

While the discussion above has been focused on the last part of the reaction path of both pigments (from −40° to −80° Rh and from −60° to −90° for isoRh) the total changes (from the Franck−Condon point to the intersection) in the value of the dihedral angles associated with the torsion about the $-C_9$=$C_{10}-$ and $-C_{11}$=$C_{12}-$ reactive bonds, are given in Table 1. From Table 1 and Figure 2, it is also apparent that there are other (lesser) torsional deformations that contribute to the S_1 reaction coordinate of Rh and isoRh. For instance, in both pigments, the $-C_{13}$=$C_{14}-$ double bond undergoes a ∼+20° increase from the Franck−Condon point to the conical intersection.

4. Conclusions

The computational investigation of a photochemical reaction in the protein environment is currently a formidable research target. A primary requirement to be fulfilled is the accurate mapping of the force field (i.e., of the potential energy surface) driving the reaction. In the present contribution, we have provided evidence that a CASPT2//CASSCF/6-31G*/AMBER strategy can be used to study the structure of a rather wide region of the excited-state potential energy surface of visual pigments spanning the Rh and isoRh analogues (isoRh can be seen as a diastereoisomer of Rh). These results provide an unprecedented

(38) Warshel, A.; Barboy, N. *J. Am. Chem. Soc.* **1982**, *104*, 1469−1476.
(39) Cooper, A. *FEBS Lett.* **1979**, *100*, 382−384.
(40) Randall, C. E.; Lewis, J. W.; Hug, S. J.; Björling, S. C.; Eisner-Shanas, I.; Friedman, N.; Ottolenghi, M.; Sheves, M.; Kliger, D. S. *J. Am. Chem. Soc.* **1991**, *113*, 3473−3485.
(41) Spalink, J. D.; Reynolds, A. H.; Rentzepis, P. M.; Sperling, W.; Applebury, M. L. *Proc. Natl. Acad. Sci. U.S.A.* **1983**, *80*, 1887−1891.

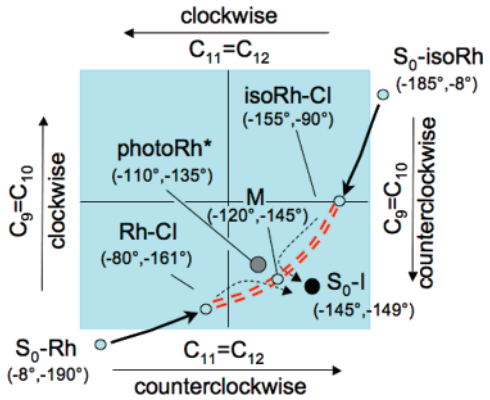

Figure 6. Topography of the excited-state potential energy surface of the visual pigment. The dashed lines indicate the intersection space connecting the **S_0-Rh → Rh−CI** and **S_0-isoRh → isoRh−CI** paths. The * indicates the experimentally derived structure of ref 16. The values in parenthesis refer to the $C_{10}-C_{11}-C_{12}-C_{13}$ and $C_8-C_9-C_{10}-C_{11}$ dihedral angles, respectively. Notice that the S_0 photoRh intermediate (probably a vibrationally hot transient species[1,16] of bathoRh) is expected to have bond lengths close to the ones of **S_0-I** (e.g., 1.36, 1.46, 1.35 Å for the $C_9-C_{10}-C_{11}-C_{12}$ segment) and very different from the ones of **M** (e.g., 1.44, 1.35, 1.48 Å for the $C_9-C_{10}-C_{11}-C_{12}$ segment) or of other conical intersection points.

"wide angle" view of the excited-state potential energy structure that is schematically illustrated in the diagram of Figure 6.

According to the energy profiles of Figure 2, the relaxation of Rh and isoRh from their Franck−Condon point toward the S_1/S_0 intersection is driven by a 15 and 22 kcal mol^{-1} excess energy, respectively. Thus, remarkably, the longer living (100 fs fluorescence lifetime[42]) isoRh pigment has more vibrational excess energy available than the shorter living Rh (50 fs fluorescence lifetime[42]). The slower excited-state dynamics of isoRh may be associated with the existence along the S_1 relaxation path of a deeper energy minimum (at −50°). Alternatively, for the case of Rh, trajectory computations[21] indicate that a shallow energy minimum (e.g., at −30° in Figure 2) does not affect the excited-state dynamics. Thus, the isoRh slower dynamics and, consequently, the slower photoproduct appearance time of isoRh (600 fs) with respect to Rh (200 fs)[43] cannot be explained on the only basis of the structure of the S_1 reaction paths. The observed presence of vibrational excess energy as well as non-stationary vibrational states in the two pigments is also in line with the results of the same Rh trajectory[21] computation that reveals a ∼10 kcal mol^{-1} increase in the S_1-S_0 energy gap in the 30°−40° region. This would set the fluorescence maxima predicted for both Rh and isoRh (that have S_1-S_0 energy gap ∼33 kcal mol^{-1} excitation energies in Figure 4B at −30°) to ∼43 kcal mol^{-1} falling in the observed broad excitation wavelength-dependent fluorescence bands centered in the 600−700 nm region.

As described above and illustrated in Figure 6, the evolution of the **S_0-isoRh** structure along the reaction coordinate leads directly toward the **S_0−Rh** structure and vice versa. According to our reaction coordinate analysis, this motion is associated with a mechanism based on an asynchronous clockwise/counterclockwise torsional deformation of the $-C_{11}=C_{12}-/-C_9=C_{10}-$ bonds in the **S_0-isoRh → S_0-Rh** direction and a reversed counterclockwise/clockwise deformation in the **S_0-Rh → S_0-isoRh** direction. It shall be noted that these mechanisms are a generalization of the bicycle pedal mechanism originally proposed by Warshel[3] on the basis of a semiempirical quantum chemical model of Rh and only recently confirmed via scaled-CASSCF/AMBER trajectory computations on the **S_0-Rh** model.[21] Also notice that, as apparent from Figure 5 and Table 1, more moderate changes of other torsional angles follow the two paths. This includes, in both pigments, the $-C_{13}=C_{14}-$ double bond that constitutes the reactive bond in microbial rhodopsins (e.g., in bacteriorhodopsin).

It is informative to follow the evolution of the $C_{10}-C_{11}-C_{12}-C_{13}$ and $C_8-C_9-C_{10}-C_{11}$ dihedral angles (i.e., of the torsional deformation of the $-C_{11}=C_{12}-$ and $-C_9=C_{10}-$ bonds) along the converging paths. As stressed above and shown in Figure 6, the excited-state evolution of both pigments points toward the same intersection space segment. This region, that has been investigated in a previous report,[44] would constitute the bottom of a single S_1 potential energy valley connecting the **S_0-Rh** and **S_0-isoRh** Franck−Condon points. Interestingly, the experimentally derived values of the $C_{10}-C_{11}-C_{12}-C_{13}$ and $C_8-C_9-C_{10}-C_{11}$ dihedrals for photorhodopsin (photoRh), that is the primary (non-isolable) photoproduct of Rh and precursor of bathoRh,[1,2] place this critical structure close to the intersection space segment (e.g., to a conical intersection point **M** located almost halfway between **Rh−CI** and **isoRh−CI**). Of course, this does not mean that photoRh is a point of the intersection space (most likely, it would differ in the value of the double-bond expansion/single-bond contraction coordinate of the branching space[44] leading far from the S_1/S_0 degeneracy. See also the figure legend) but suggests that can be impulsively populated by continuing the evolution along the **S_0-Rh → Rh−CI** direction and after decaying at **Rh−CI**. It is also interesting that, consistent with the diagram in Figure 6, in order to populate the bathoRh valley (centered at **S_0-I**) the average direction of that structural evolution must change. In fact, bathoRh could be effectively populated only if the system (i.e., the center of the vibrational wavepacket), after achieving the photoRh configuration, reverts the $-C_8-C_9-C_{10}-C_{11}-$ dihedral angle change, moving in an almost orthogonal (i.e., weakly coupled) mode. This change in motion could be the origin of the picosecond time scale required for generation of bathoRh from photoRh.[16,45]

In spite of several recent computational studies on the photoinduced isomerization of visual pigments, two key features currently remain to be understood. The first regards the nature of photoRh, an elusive intermediate, that no computational study has been able to model. The second and more fundamental point regards the molecular factor at the basis of the high quantum yield of Rh (67%) with respect to that of isoRh (22%). While it is likely that the understanding of the structure of the energy surfaces of these molecules constitutes a prerequisite for the solution of these problems, this cannot be provided by the present knowledge. In this case, the calculation of a suitable set of trajectories is required.[46] As suggested by recent trajectory studies on reduced PSB11 models,[47] as well as anticipated by

(42) Kochendoerfer, G. G.; Mathies, R. A. *J. Phys. Chem.* **1996**, *100*, 14526−14532.
(43) Schoenlein, R. W.; Peteanu, L. A.; Wang, Q.; Mathies, R. A.; Shank, C. V. *J. Phys. Chem.* **1993**, *97*, 12087−12092.
(44) Migani, A.; Sinicropi, A.; Ferré, N.; Cembran, A.; Garavelli, M.; Olivucci, M. *Faraday Discuss.* **2004**, *127*, 179−191.
(45) Peteanu, L. A.; Schoenlein, R. W.; Wang, Q.; Mathies, R. A.; Shank, C. V. *Proc. Natl. Acad. Sci. U.S.A.* **1993**, *90*, 11762−11766.
(46) Warshel, A.; Chu, Z. T. *J. Phys. Chem. B* **2001**, *105*, 9857−9871.
(47) Weingart, O.; Schapiro, I.; Buss, V. *J. Phys. Chem. B* **2007**, *111*, 3782−3788.

experimental studies,[16] other modes such as the HOOP vibrational modes accompanying the isomerization motion may play a fundamental role in these processes.

Acknowledgment. We thank CINECA for granted calculation time, Fondazione Monte dei Paschi di Siena and the University of Siena, PAR Progetti 2005 for generous funding. M.O. is grateful to the Center for Photchemical Sciences and the College of Arts and Sciences for start-up funding. P.B.C. and L.M.F. are grateful for a Postdoctoral fellowship of the Ministerio de Educación y Ciencia of Spain. P.C.B. acknowledges the funding from a contract of the Juan de la Cierva programme from the Spanish MEC/FEDER CTQ2004-01739 and CTQ2007-61260 projects and from the Generalitat Valenciana GV06-192 project.

Supporting Information Available: Details of the QM/MM scheme; coordinates of all optimized structures; tables of energies, charge distribution, $\Delta\mu$ and f; comparison with experimental data; bare chromophore scan; complete torsional motion; and complete ref 26. This material is available free of charge via the Internet at http://pubs.acs.org.

JA0749082